McsB regulates CtsR thermosensing through periphery arginine phosphorylation

Huahuan Cai[a,1], Boyang Hua[b,c,1,2], Yeting Guo[a,d], Xing-Hua Xia[b,c,2], Yufen Zhao[a,e,f,2]

[a]Institute of Drug Discovery Technology, Ningbo University, Ningbo 315211, China
[b]School of Chemistry and Chemical Engineering, Nanjing University, Nanjing 210023, China
[c]State Key Laboratory of Analytical Chemistry for Life Sciences, Nanjing University, Nanjing 210023, China
[d]Institute of Biophysics, College of Life Sciences, Zhejiang University, Hangzhou 310058, China
[e]Department of Chemical Biology, College of Chemistry and Chemical Engineering, Xiamen University, Xiamen 361005, China
[f]Key Laboratory of Bioorganic Phosphorus Chemistry and Chemical Biology (Ministry of Education), Department of Chemistry, Tsinghua University, Beijing 100084, China

[1]H.C. and B.H. contributed equally to this work.
[2]To whom correspondence may be addressed.

Author contributions
H.C. and B.H. designed the research; H.C., B.H., and Y.G. performed experiments and analyzed data; H.C., B.H., X.X., and Y.Z. wrote the paper; B.H., X.X., and Y.Z. funded and supervised the project.

Conflict of interests
The authors declare no competing interest.

Abstract

Post-translational protein modifications (PTMs) are a ubiquitous phenomenon that exists in all domains of life. The bacterial transcription repressor CtsR becomes phosphorylated by the arginine kinase McsB when cells sense an elevated temperature in the environment. Here, we perform single-molecule experiments based on the protein-induced fluorescence enhancement (PIFE) effect to monitor the DNA-CtsR-McsB interaction. Our single-molecule analysis reveals that CtsR binds rapidly and stably to the cognate DNA, and that McsB transiently interacts with the DNA-bound CtsR. We determined the binding kinetics between McsB and the DNA-bound CtsR by single-molecule real-time binding assays, with k_{on} and k_{off} of 0.80 μM^{-1} s^{-1} and 0.14 s^{-1}, respectively. Through this interaction, McsB does not remove CtsR from the DNA, but instead alters its thermosensing behavior, lowering the temperature threshold for CtsR dissociation. Phosphorylation of several periphery arginine residues on CtsR underlies a plausible molecular mechanism for this effect. Taken together, these results provide insights into how CtsR might integrate inputs from different environment stresses and regulate the initiation of the heat-shock response when cells are faced with complex environment conditions.

Introduction

First discovered in 1976, arginine phosphorylation is a widespread and crucial PTM in both prokaryotic and eukaryotic cells.[1,2] It is estimated that over 10,000 phosphorylated arginine sites exist in the bacterial and human proteomes, showcasing the scale and prevalence of this form of N-phosphorylation.[3-7] Arginine phosphorylation on a protein can influence its structure, activity, stability, interactions and cellular localizations. In bacteria, numerous important biological processes are influenced by this PTM, such as gene expression regulation[8,9] and cell division,[10] highlighting its broad roles in bacterial adaptation, persistence, and virulence.[11-15] Despite the importance of this PTM, the identity of the kinase responsible for phosphorylating arginine residues remained elusive for a long time.

McsB is the founding member of the cellular arginine kinases and is shown to phosphorylate several arginine residues on the bacterial master transcription repressor CtsR.[9] Recent structural studies reveal that McsB has an N-terminal phosphagen kinase (PhK)-like phosphotransferase domain and a C-terminal dimerization domain containing a phospho-arginine-binding pocket.[16] McsB typically functions as a multimer, ranging from dimers in *Geobacillus stearothermophilus* to mostly higher-order oligomers in *Bacillus subtilis*.[17] The state of oligomerization is thought to regulate the kinase activity of McsB, since mutations that disrupt the dimer formation markedly reduce the activity.[16] McsB autophosphorylation is important to its function, as the dimerization process is mediated through the phospho-arginine residues.[16,17] Besides the autophosphorylation and oligomerization, the kinase activity of McsB in *B. subtilis* also requires the cofactor McsA, which enhances the kinase activity of McsB by reorganizing the catalytic site, accelerating the enzyme's turnover rate, and increasing its thermostability.[18,19]

The McsB-CtsR system plays an indispensable role in the cellular responses to harsh conditions and promote cell survival under stress situations, such as the heat, oxidative, and metal ion stresses.[9,20-24] For example, in Gram-positive bacteria, the heat stress causes protein misfolding-induced toxicity and triggers protein quality control responses mediated by the transcription repressors HcrA and CtsR.[21,25-28] Under normal conditions, CtsR forms a dimer that specifically binds to the promoter region of the *clpC* operon and represses the expression of the operon which includes several heat-shock response genes, such as *ctsR*, *mcsA*, *mcsB* and *clpC* in *B. subtilis*.[29] Based on previous structural studies, the CtsR dimer interacts with DNA mainly through its several arginine residues, with R28 and R49 bind the major groove whereas R62 invades deeply in the minor groove.[9] Upon heat exposure, a glycine-rich loop in CtsR senses the temperature change and promotes CtsR dissociation from the DNA, thus activating the expression of the *clpC* operon.[30] Once dissociated, R28, R49 and R62 become exposed and are phosphorylated by the arginine kinase McsB. Arginine phosphorylation inverses the charges on the arginine residues and prevents its interaction with the negatively charged DNA backbones.[9] Furthermore, arginine phosphorylation also signals for protein degradation by the ClpCP protease system in the prokaryotes, akin to the function of ubiquitination in the eukaryotes.[31]

Apart from the three core arginine residues mentioned above (R28, R49 and R62), it was shown that McsB can phosphorylate five other arginine residues on CtsR (*i.e.*, the periphery arginine residues),[9] although it is unclear if their phosphorylation affects the CtsR-DNA binding affinity. To address this question, we employed several single-molecule fluorescence techniques to study how McsB regulates CtsR and its temperature-dependent DNA binding affinity. The toolbelt of single-molecule fluorescence techniques, which commonly include colocalization,[32] fluorescence resonance energy transfer (FRET)[33,34] and PIFE[35,36] methods, are now routinely applied in biological studies. Due to the ability to reveal heterogeneous subpopulations and hidden intermediate states, these tools are ideal for studying the structural and interaction dynamics of biomolecule complexes. In this work, our single-molecule results suggest that McsB transiently interacts with the DNA-bound CtsR. This interaction, likely mediated through the periphery arginine residues on CtsR, does not directly result in the dissociation of CtsR from its target DNA, but rather renders CtsR more sensitive to heat, making the protein fall off at lower temperatures. Our findings further elaborate the function of arginine phosphorylation on CtsR and demonstrate a mechanism by which McsB influences the regulation of gene expression.

Results

First, to study the interaction between CtsR and its cognate DNA, we designed a fluorescently labeled DNA probe that exhibited the PIFE effect[36] upon CtsR binding. Briefly, a fluorophore is placed adjacent to the CtsR consensus sequence so that CtsR binding positions the protein in close vicinity to the fluorophore, resulting in a fluorescence enhancement **(Figure 1A-B)**. The fluorophore used and its labeling

position on the DNA were optimized, as these factors were shown to affect CtsR binding and the PIFE effect **(Supplementary Figure 1A-B)**. We used this DNA probe and a sequence-scrambled control to determine the binding affinity of CtsR to its target DNA. The K_D was around 10 nM for the cognate DNA whereas the non-cognate control was barely bound by CtsR even at elevated protein concentrations **(Figure 1C and Supplementary Figure 1C)**, demonstrating the high affinity and sequence specificity of the CtsR-DNA interaction. The measured K_D is in agreement with the previous result measured by isothermal titration calorimetry. Based on this result, 25 nM to 50 nM CtsR was used in most of the following experiments to ensure a saturated binding of the DNA targets.

Next, we explored the feasibility of using the PIFE reporter to monitor CtsR binding in real time. We constructed a flow cell and introduced unlabeled CtsR during live image acquisition **(Figure 1D and Supplementary Figure 1D)**. Before adding CtsR, we detected a stable and low fluorescence intensity level, corresponding to the unbound DNA probe. Upon the addition of CtsR, a single-step increase in the fluorescence intensity was observed, indicating the binding of CtsR to the target DNA. To estimate the binding rate k_{on}, we constructed a series of time-dependent intensity histograms, which showed that the binding events were largely completed within 4 s after CtsR addition **(Figure 1E and Supplementary Figure 1E)**, indicating CtsR has a rapid DNA binding rate. In most of the single-molecule trajectories, CtsR stably bound until the end of the movie or when photobleaching occurred (*e.g.*, a single-step decrease in the fluorescence intensity to the baseline level, **Figure 1D**). Only a small fraction of the molecules showed a two-step fluorescence intensity decrease which may represent CtsR dissociation (*i.e.*, the loss of PIFE) followed by photobleaching **(Supplementary Figure 1D)**. Furthermore, we did not observe CtsR dissociation after washing away CtsR in solution (**Supplementary Figure 1F**). These results suggest that CtsR has a relatively slow unbinding rate and binds stably to its target DNA. To further assess the unbinding rate beyond the limit of photobleaching, we took intensity histograms 5 min and 20 min after washing away the excess CtsR in solution. At room temperature, CtsR stayed bound to its target DNA for at least 20 min without displaying significant dissociation **(Figure 1F)**.

McsB phosphorylates several key arginine residues on CtsR, thus reversing the positive charges and impairing its binding to the negatively charged DNA.[9] To study if McsB can remove the DNA-bound CtsR in our assays, we incubated the CtsR-DNA complex with the autophosphorylated and active McsB (pMcsB) from *G. stearothermophilus*, and took intensity histograms at room temperature 5 min and 20 min after the addition of pMcsB and ATP **(Figure 2A)**. Unlike the free CtsR, which was completely inactivated by pMcsB **(Supplementary Figure 2A)**, the DNA-bound CtsR remained active and did not show any loss of PIFE that indicated its removal. Interestingly, the population of the CtsR-DNA complex shifted to slightly higher intensities after the pMcsB and ATP treatment. To rule out the possibility that CtsR was nonspecifically stuck to the surface and thus could not be removed by pMcsB, an unlabeled cognate

DNA (without biotin) was added in solution to compete with the surface-tethered DNA targets. We observed a substantial down-shift in the intensity histograms, suggesting the successful dissociation of CtsR from the surface **(Supplementary Figure 2B-C)**.

We then performed a real-time flow-in experiment to monitor the CtsR-DNA complex upon the pMcsB and ATP addition **(Figure 2B-C)**. Before the pMcsB flow-in, a stable and high intensity level was observed due to the PIFE effect caused by the bound CtsR. After the pMcsB flow-in, as sometimes marked by an abrupt defocusing and refocusing event, we detected frequent and transient fluorescence intensity increases to an even higher level beyond that induced by CtsR alone. Such fluorescence intensity increases were much less common when a buffer without pMcsB was flown in **(Supplementary Figure 2D)**. We argued that these transient fluorescence intensity increases could be the result of transient pMcsB binding events to the CtsR-DNA complex, which induced a stronger PIFE effect and was reflected in the up-shifts observed in the intensity histograms **(Figure 2A)**. For clarity, we herein refer to the phenomenon as "turbo" PIFE **(Figure 2C)**. Control experiments showed that the "turbo" PIFE effect was not due to direct interactions between pMcsB and the target DNA **(Supplementary Figure 2E)**.

To further validate the interaction between pMcsB and the DNA-bound CtsR, we made a HaloTagged McsB protein and labeled it with the Abberior STAR RED (AS RED) fluorophore. As determined by the ability to inactivate the CtsR-DNA binding, pMcsB-HaloTag was kinase-active but showed a decreased activity as compared to the untagged wild-type kinase **(Supplementary Figure 3A)**. Specific binding events of the pMcsB-HaloTag to the DNA-bound CtsR were observed, which were absent when only the non-specifically bound CtsR, if any, or the target DNA alone was on the imaging surface **(Figure 3A)**. We also performed single-molecule real-time binding assays[37] on pMcsB-HaloTag with the surface-tethered CtsR-DNA complex **(Figure 3B)**. Following the flow-in of pMcsB-HaloTag, it began to bind transiently and repeatedly to the same locations (with a radius < 40 nm), indicating specific and transient binding of pMcsB to the same CtsR-DNA complexes. Based on the fluorescence intensity trajectories we obtained, the k_{on} and k_{off} rates of pMcsB-HaloTag were estimated to be 0.80 μM^{-1} s^{-1} and 0.14 s^{-1}, respectively **(Supplementary Figure 3B-C)**.

In previous mass spectroscopy (MS) and protein mutant studies, 8 arginine residues on CtsR can be phosphorylated by McsB. Among these 8 residues, 3 arginine residues establish substantive interactions with the DNA major and minor grooves (R28, R49 and R62, *i.e.*, the core arginine residues).[9] Phosphorylation or phospho-mimic mutations of these key arginine residues, especially R62, completely abolishes the DNA binding activity of CtsR.[9] In our results, CtsR stayed bound to the DNA during its interaction with pMcsB **(Figure 2)**, indicating the interactions between the core arginine residues and the DNA were largely unaffected. To determine which arginine residues are phosphorylated by pMcsB upon its interaction with the CtsR-DNA complex, we conducted liquid chromatography (LC)-MS/MS experiments. Briefly, CtsR without and with different amounts of DNA were reacted with pMcsB and ATP at

42˚C. The reaction solutions were processed and digested to generated the tryptic peptides for LC-MS/MS analysis. For the CtsR sample without DNA, we were able to detect peptides containing phosphorylated arginine residues at positions 49, 62, 36, 54 and 69. However, with increasing amounts DNA, the relative spectral counts for phosphorylated peptides containing R49 and R62 decreased and became undetectable at the highest DNA:CtsR ratios, whereas the relative spectral counts for phospho-R36, R54 and R69-containing peptides were largely unchanged **(Figure 3C)**. This observation indicates that the periphery arginine residues can be phosphorylated by McsB in the presence of DNA, and is in agreement with the previous results that the DNA-bound CtsR exhibits a reduced rate of phosphorylation at the core arginine residues by McsB, possibly because these residues are deeply buried and protected from the kinase by the DNA backbones.

Based on the MS results, we therefore hypothesize that pMcsB mainly interacts with the DNA-bound CtsR through the periphery arginine residues that are exposed to solution. To test this hypothesis, we made a CtsR-3RK mutant in which three periphery arginine residues (R36, R54 and R69) were mutated to lysine. CtsR-3RK bound to the DNA target with a moderately reduced affinity, possibly due to its slightly perturbed structure upon mutation **(Supplementary Table 1A)**, but the majority of CtsR-3RK remained bound to the DNA 5-10 min after the excess protein in solution was washed away **(Supplementary Figure 3D)**. In contrast to the wild-type CtsR, the 3RK mutations completely abolished the interaction between the DNA-bound CtsR and pMcsB-HaloTag **(Figure 3D)**. Although we cannot rule out that the structural perturbations caused by the mutations played a role (see **Discussion**), this result suggests that the CtsR-McsB interaction observed above is mainly mediated through the periphery arginine residues.

We then explored the potential biological effects on the CtsR-DNA complex caused by its interaction with pMcsB. Previous studies demonstrate that the glycine-rich loop in CtsR acts as a temperature sensor and regulates the CtsR-DNA binding affinity in response to temperature changes.[30] Without the help of McsB, sufficiently elevated temperatures alone can dissociate CtsR from its target DNA. To test this in our experiments, we flowed in a heated buffer in the flow cell, which subjected the CtsR-DNA complex to elevated temperatures and quickly washed away the dissociated CtsR to prevent rebinding **(Supplementary Figure 4A)**. The CtsR-DNA complex was stable and tolerated pulses of heated buffer washes up to 42˚C **(Figure 4A)**. We wonder if treating the CtsR-DNA complex with pMcsB could alter its tolerance to elevated temperatures. After pre-treating the DNA-bound CtsR with pMcsB and ATP for 10 min, CtsR became susceptible to heated buffer washes at the temperature of 42˚C **(Figure 4B)**. We tried to exclude pMcsB and ATP in the heated washing buffer, with the reason that including pMcsB in the heated buffer could introduce additional effects that only occurred between CtsR and pMcsB at the higher temperatures. The results showed that even when pMcsB was removed prior to the temperature jump and excluded from the heated washing buffer, the pre-treated CtsR was still heat-susceptible at 42˚C **(Figure**

4C). To test if this effect was related to phosphorylation, the CtsR-DNA complex was treated with McsB (not the auto-phosphorylated pMcsB) in the absence of ATP. Pre-treating the CtsR-DNA complex in the absence of ATP did not lead to the heat-sensitization of CtsR, as buffer washes at 42˚C did not induce CtsR dissociation **(Figure 4D)**. Therefore, it is likely that the pre-incubation with pMcsB and ATP rendered the DNA-bound CtsR more heat-sensitive through arginine phosphorylation, which may explain why the R49 and R62 phosphorylation became undetectable only at DNA:CtsR ratios far beyond the stoichiometry (*i.e.*, 0.5:1), in which case the large excess of DNA and its fast CtsR binding rate kinetically competed and blocked McsB from phosphorylating R49 and R62.

Discussion

Since both the PhK-like phosphotransferase and the phospho-arginine-binding domains are capable of binding (phospho-)arginine residues,[16] it is not clear which domain(s) on McsB is responsible for interacting with the DNA-bound CtsR. Our single-molecule analysis suggests that both domains may play a role in facilitating the CtsR-McsB interaction. In **Supplementary Figure 3B**, during the first 3 min after the pMcsB-HaloTag flow-in, most of the McsB binding events were transient, with very few events lasting longer than 40 s (2%). However, after 5-7 min incubation with pMcsB, an increased population of the CtsR-DNA complex became stably bound by pMcsB (>40 s, 21%, **Supplementary Figure 3E**). This stably bound population of McsB could explain how a further up-shift in the intensity histograms occurred after 20 min incubation of CtsR with pMcsB, as compared to 5 min incubation **(Figure 2A)**. Based on the two modes of binding events, we reason that, when CtsR is not phosphorylated initially, McsB mainly interacts with it transiently through the PhK-like kinase domain. After CtsR becomes phosphorylated, it can interact more stably with McsB through the phospho-arginine binding pocket.

To understand how periphery arginine phosphorylation could make CtsR more sensitive to heat, we used AlphaFold3[38] to predict the structure of the complex formed between CtsR and the target DNA. Because arginine phosphorylation is not available in the model of AlphaFold3, we chose the arginine-to-aspartic acid mutation as a mimic of arginine phosphorylation. All the mutants we examined, including the CtsR-3RK mutant mentioned above, displayed a RMSD of less than 0.5 Å as compared to the wild-type CtsR structure, suggesting that the point mutations had a minimal effect on protein folding **(Supplementary Figure 4B and Supplementary Table 1A)**. To estimate and compare the binding strength of the various CtsR-DNA complexes, we characterized the hydrogen bonds formed between the DNA and CtsR or its phospho-mimic mutants **(Supplementary Table 1B)**. For instance, the wild-type CtsR formed 21 pairs of hydrogen bonds with the DNA. The triple phospho-mimic mutant of the three core arginine residues (R28, R49 and R62) led to a drastic weakening in hydrogen bonding, forming only 15 pairs, whereas mutations of the three periphery arginine residues (R36, R54 and R69) only modestly diminished the strength of the complex, forming 21 pairs of hydrogen bonds but with a slightly longer average bond length **(Supplementary**

Figure 4C and Supplementary Table 1B). The other 6 possible single and double phospho-mimic mutants of R36, R54 and R69 were also examined, all of which were observed to form 21 pairs of hydrogen bonds with almost identical average bond length to the wild-type complex. Although predicting protein folding and interactions with the phospho-mimic mutations cannot fully recapitulate the effects caused by adding phosphate groups on a folded structure (*e.g.*, due to kinetic reasons), these results shown here partly explained how periphery arginine phosphorylation modulated the strength of the CtsR-DNA interaction.

In comparison to the colocalization and FRET assays, PIFE requires a minimum of one excitation and emission channel in the microscope, making the instrument easier to build and more accessible. Besides, another benefit of the PIFE assay is that it can work with unlabeled proteins, circumventing the "concentration barrier" of detecting single-molecule signals when a high concentration of fluorescently labeled species is present in the solution (*e.g.*, 200 nM McsB, **Figure 2**).[39] Although the PIFE effect is thought to occur when the protein and fluorophore are within a short distance range (*e.g.*, 1-2 nm),[36] our results demonstrated that, with a proper design of the fluorescent probe, PIFE can be sensitive not only to the presence of direct protein partners (*e.g.*, CtsR, **Figure 1**), but also to indirect and secondary interactions (*e.g.*, McsB, **Figure 2**), making PIFE a versatile tool for studying protein-nucleic acid interactions. In practice, since a protein can exert rather complex effects on the fluorophore, the choice of the fluorophore and its labeling position need to be optimized on a protein-specific basis as outlined in this and previous studies.[40]

Our results show that the CtsR-DNA complex is stable and forms transient interactions with McsB at room temperature. Although McsB does not directly dissociate CtsR from the complex, it leaves phosphorylation marks on several periphery arginine residues and lowers the temperature threshold for CtsR dissociation. Different from the previous model where McsB plays a passive role in regulating CtsR by inactivating the protein only after it dissociates from the DNA, our findings suggest that McsB may also actively modify the phosphorylation states of the DNA-bound CtsR *in situ* in response to the outside environment **(Figure 4E)**. We reason that the phosphorylation states of the periphery arginine residues could help integrate inputs from environmental stresses and determine the proper temperature threshold at which cells initiate the heat-shock response. In bacteria, the phosphorylation states of CtsR are combinedly regulated by the kinase McsB and phosphatase YwlE,[10,41] which dynamically add and remove phosphorylation marks, respectively. The balance between the enzyme pair is vital to the precise control of the related cellular functions and gene expression regulation. It is known that certain stresses, such as the oxidative stress, inactive the phosphatase YwlE by causing the formation of disulfide bonds within the enzyme,[21] which results in accumulated phosphorylation modifications on CtsR. In our model, when bacteria are already faced with a mild oxidative stress, the cells might tune its heat tolerance threshold and initiate the heat-shock response at a lower temperature, as a way to protect the cells from extensive damages in a harsh environment of multiple stresses.

Materials and Methods

Protein over-expression and purification

The plasmid for *G. stearothermophilus* McsB was a gift of Tim Clausen. The plasmids for *G. stearothermophilus* CtsR and CtsR-3RK, recombinant McsB-HaloTag were synthesized by SYNBIO Technologies. In general, protein over-expression was performed in *Escherichia coli* BL21(DE3) grown in LB-medium supplemented with 50 μg/ml carbenicillin. The cultures for McsB and McsB-HaloTag were grown to an OD600 of 1.0 at 37˚C, and 0.5 mM IPTG was added and the culture was shifted to 18˚C for overnight expression. The cultures for CtsR and CtsR-3RK were grown to an OD600 of 0.8 at 37˚C, followed by induction with 1 mM IPTG for 4 h. Cells were harvested and the pellet was resuspended in lysis buffer (50 mM PBS, pH 7.5 and 150 mM NaCl, 10% glycerol, 1 mM 2-mercaptoethanol, 1 mM PMSF). All proteins were purified by Ni-NTA affinity chromatography using a 1 mL His Trap column (GE Healthcare Life Science). The column was equilibrated with balance buffer (50 mM PBS pH 7.5 and 150 mM NaCl, 10% glycerol, 50 mM imidazole). Bound proteins were eluted in gradient buffer (Buffer A: 50 mM PBS, pH 7.5, 150 mM NaCl, Buffer B: 50 mM PBS, pH 7.5, 500 mM NaCl, 500 mM imidazole). The proteins were further purified by a Superdex 200 column (GE Healthcare Life Sciences) equilibrated with the balance buffer (50 mM PBS pH 7.5, 150 mM NaCl). Finally, the proteins were concentrated by a 10 kDa Amicon Ultra-0.5 mL centrifugal filter (Millipore) and stored at -80˚C for storage.

Protein labeling

The McsB-HaloTag protein was labeled with the Abberior® STAR RED HaloTag® Ligands (Abberior) following the manufacture's procedures. The labeled protein was loaded to a column (Beyotime Biotechnology) to remove the excess fluorophore. Labeling efficiency was calculated according to the maximum absorption of the protein and the fluorophore.

Mutagenesis

Site-directed mutagenesis of *G. stearothermophilus* CtsR expression constructs were performed using the PrimeSTAR HS DNA Polymerase (Takara) following the manufacturer's procedures. Primers are listed in **Supplementary Table 2**.

McsB (auto)phosphorylation assay

The McsB or McsB-HaloTag (10 μM) autophosphorylation reaction was performed in 30 mM Tris-HCl pH 7.4, 20 mM KCl, 5 mM $MgCl_2$, and 1 mM ATP at 42˚C for 5 min.

To phosphorylate CtsR in solution, 200 nM pMcsB or pMcsB-HaloTag was incubated with 50 nM CtsR in the reaction buffer (30 mM Tris-HCl pH 7.4, 20 mM KCl, 5 mM $MgCl_2$, and 0.5 mM ATP) at 25˚C for 15 min. CtsR phosphorylation was monitored by single-molecule PIFE assays.

AlphaFold3 simulation

The structure of the CtsR-DNA complex was predicted using the AlphaFold server, with the number of protein copies set to 2. The DNA binding sequence (26 bp) is provided in **Supplementary Table 2**. Random seed values were fixed at 1 for the prediction. Aspartic acid was used as a substitute to mimic the phosphorylated arginine (CtsR-RD) on CtsR. The CtsR-RD-DNA complexes were similarly predicted using the AlphaFold server, employing identical settings to those used for the wild-type complex.

Mass spectroscopy of arginine residues on CtsR

CtsR (2 μg) was pre-incubated with various amounts of the 26-bp DNA substrate for 5 min in Tris-HCl buffer (pH 8.0) containing 100 mM KCl, 5 mM $MgCl_2$ and 1 mM ATP. Subsequently, 2.1 μg of McsB was added to the binding solution, and the mixture was incubated at 42˚C for 1 h. The reacted CtsR (600 ng) was treated with 8 M urea at room temperature for 30 min, followed by reduction with 10 mM tris(2-carboxyethyl) phosphine (TCEP, thermos Fisher Scientific) at 37˚C for 40 min. Alkylation was performed with 25 mM iodoacetamide (IAA, thermos Fisher Scientific) at room temperature for 25 min. The solution was then loaded onto a home-made tip equipped with a 10 kDa filter and centrifuged to remove urea, as well as the excess TCEP and IAA.[42] The tip was washed three times with 50 mM ammonium bicarbonate (ABC) before trypsin solution (Promega) was added. Digestion was carried out in a 37˚C water bath overnight.

For LC-MS Analysis, an UltiMate™ NCS-3500RS nano system was coupled to an Orbitrap Fusion Lumos Tribrid mass spectrometer (Thermo Fisher Scientific) for peptide analysis. Peptides were eluted using a binary gradient of buffer A (0.1% (v/v) formic acid) and buffer B (100% (v/v) acetonitrile) over a 60-minute period. The gradient progressed from 98% buffer A and 2% buffer B to 35% buffer B at a flow rate of 0.35 μL/min. The mass spectrometer was operated in data-dependent acquisition mode, beginning with a full scan (m/z range 375–1800). The Orbitrap resolution for MS/MS scans was set to 15,000, with a cycle time of 2 seconds (isolation width: 1.6 m/z, mass tolerance: 10 ppm). Precursor ions with charge states of 2–7 were selected for fragmentation and placed on a dynamic exclusion list for 30 seconds. The minimum intensity threshold for precursor selection was set to 5×10^4. Fragmentation was performed using higher-energy collisional dissociation (HCD) with a normalized collision energy of 30%. Additionally, the AGC (Automatic Gain Control) target was set to a custom model, and the maximum injection time was configured to 25 ms.

Raw data were analyzed using Proteome Discoverer (version 2.3.0.523, Thermo Scientific) against a combined database consisting of the UniProt Reference Proteome of *E. coli* strain BL21(DE3), common contaminants, and the sequences of *G. stearothermophilus* CtsR and McsB. Methylthio-modification of cysteine was specified as a fixed modification, while phosphorylation of Arg, Lys, His, Ser, Thr, and Tyr, as well as oxidation of Met, were set as dynamic modifications. Due to the impaired tryptic cleavage at phosphorylated arginine, up to three missed cleavage sites were permitted.

The peptide mass tolerance was set to 5 ppm, and the fragment ion mass tolerance to 0.02 Da. Quantitative information for CtsR peptide spectrum matches (PSMs) was obtained through spectral counting. At each arginine residue, the spectral counts of phosphorylated and total peptides containing that residue were calculated.

Bulk fluorescence measurements

The measurements were performed in a Fluorescence Spectrophotometer F-7100 (Hitachi High-Technologies). The samples were excited with a 520 nm and 650 nm wavelength for Cy3 and Cy5, respectively. To measure the fluorescence spectra, a 1X1 cm Quartz cuvette was filled with 2 nM fluorophore-labeled DNA, followed by adding CtsR to the specific concentrations.

Single-molecule sample preparation

To construct the fluorescently labeled DNA probe, we ordered the DNA oligos with amine modifications from Sangon Biotech., as listed in **Supplementary Table 2**. The NHS ester derivatives of non-sulfonated Cy3, sulfonated Cy3 and sulfonated Cy5 were purchased from Lumiprobe. The oligo labeling reaction was performed in 50 mM HEPES pH 7.4, 150 mM KCl. The excess fluorophores were removed with the oligo clean and concentrator kits (Zymo Research). The oligos were annealed in the same buffer as the labeling buffer.

Single-molecule data acquisition and analysis

The single-molecule imaging system was based on an objective-type total internal reflection fluorescence (TIRF) microscope (Nikon, Eclipse Ti-E). To excite the Cy3 and AS RED fluorophores, a 532-nm laser (Changchun New Industries Optoelectronics Technology, MGL-S-532-B) and a 637-nm laser (Changchun New Industries Optoelectronics Technology, TEM-F-637) were combined with a dichroic mirror (Chroma, ZT543rdc-UF1). The fluorescence emission was collected by an oil immersion objective (Nikon, CFI Apochromat TIRF 100XC) and recorded by a qCMOS camera (Hamamatsu, QRCA-Quest C15550-20UP). Two notch filers (Chroma ZET532nf and ZET635nf) were used to reject the 532-nm and 637-nm excitation lasers, respectively. A motorized xy-stage (Sanying MotionControl Instruments, PMC400) and a z-motor (Prior Scientific, ES10ZE) were used to stabilize and automate the imaging acquisition process.

To alleviate photobleaching and blinking of fluorophores, the imaging buffer (buffer containing 4 mM Trolox, 0.8% (w/v) glucose, 165 U/ml glucose oxidase and 2170 U/ml catalase) was prepared according to ref. 43.

The imaging surfaces used in this study were prepared according to ref. 44.

The single-molecule movies were analyzed according to refs. 37,44 by custom MatLab and Python codes, which are available upon request.

Acknowledgments
We thank all members of the Boyang Hua group and the Yufen Zhao group, especially Prof. Zhenbin Zhang, Dr. Yang Li and associate Prof. Songsen Fu for their technical support in MS analysis. Besides, we acknowledge the Analysis Center of Institute of Drug Discovery Technology for collecting MS data, and Tim Clausen for gifting the plasmid of *G. stearothermophilus* McsB. This work was supported by the National Natural Science Foundation of China No. 42388101 and No. 92256203 (to Y.Z.), Ningbo Top Talent Project No. 215-432094250 (to Y.Z.), State Key Laboratory of Analytical Chemistry for Life Science, Nanjing University 5431ZZXM2403 (to B.H.), and the Fundamental Research Funds for the Central Universities 2024300410 (to B.H.).

References
1. S. J. Humphrey, D. E. James, M. Mann, Protein Phosphorylation: A Major Switch Mechanism for Metabolic Regulation. *Trends Endocrinol. Metab.* **26**, 676−687 (2015).
2. M. J. Suskiewicz, T. Clausen, Chemical Biology Interrogates Protein Arginine Phosphorylation. *Cell Chem. Biol.* **23**, 888−890 (2016).
3. Y. Hu *et al.*, Bis(zinc(II)-dipicolylamine)-functionalized sub-2μm core-shell microspheres for the analysis of N-phosphoproteome. *Nat. Commun.* **11**, 6226 (2020).
4. A. Schmidt *et al.*, Quantitative phosphoproteomics reveals the role of protein arginine phosphorylation in the bacterial stress response. *Mol. Cell. Proteomics* **13**, 537−550 (2014).
5. D. B. Trentini, J. Fuhrmann, K. Mechtler, T. Clausen, Chasing Phosphoarginine Proteins: Development of a Selective Enrichment Method Using a Phosphatase Trap. *Mol. Cell. Proteomics* **13**, 1953−1964 (2014).
6. S. Fu *et al.*, Widespread arginine phosphorylation in human cells-a novel protein PTM revealed by mass spectrometry. *Sci. China Chem.* **63**, 341−346 (2020).
7. X. Chang, Y. Zhu, Y. Chen, L. Li, DeepNphos: A deep-learning architecture for prediction of N-phosphorylation sites. *Comput. Biol. Med.* **170**, 108079 (2024).
8. K. Jung, H. Jung, A new mechanism of phosphoregulation in signal transduction pathways. *Sci. Signal.* **2**, pe71 (2009).
9. J. Fuhrmann *et al.*, McsB Is a Protein Arginine Kinase That Phosphorylates and Inhibits the Heat-Shock Regulator CtsR. *Science* **324**, 1324−1327 (2009).
10. A. K. Elsholz *et al.*, Global impact of protein arginine phosphorylation on the physiology of Bacillus subtilis. *Proc. Natl. Acad. Sci. U. S. A.* **109**, 7451−7456 (2012).
11. E. Kruger, D. Zuhlke, E. Witt, H. Ludwig, M. Hecker, Clp-mediated proteolysis in Gram-positive bacteria is autoregulated by the stability of a repressor. *EMBO J.* **20**, 852−863 (2001).
12. J. Zhang *et al.*, Arginine kinase McsB and ClpC complex impairs the transition to biofilm formation in Bacillus subtilis. *Microbiol. Res.* **292**, 127979 (2024).
13. D. Frees *et al.*, Clp ATPases are required for stress tolerance, intracellular replication and biofilm formation in Staphylococcus aureus. *Mol. Microbiol.* **54**, 1445−1462 (2004).
14. N. E. M. de Oliveira *et al.*, clpB, a class III heat-shock gene regulated by CtsR, is involved in thermotolerance and virulence of Enterococcus faecalis. *Microbiology*

(Reading) **157**, 656−665 (2011).
15. D. J. Wozniak, K. B. Tiwari, R. Soufan, R. K. Jayaswal, The mcsB gene of the clpC operon is required for stress tolerance and virulence in Staphylococcus aureus. *Microbiology (Reading)* **158**, 2568−2576 (2012).
16. M. J. Suskiewicz *et al.*, Structure of McsB, a protein kinase for regulated arginine phosphorylation. *Nat. Chem. Biol.* **15**, 510−518 (2019).
17. B. Hajdusits *et al.*, McsB forms a gated kinase chamber to mark aberrant bacterial proteins for degradation. *Elife* **10**, e63505 (2021).
18. K. Lu *et al.*, Complex structure and activation mechanism of arginine kinase McsB by McsA. *Nat. Chem. Biol*. (2024).
19. M. Arifuzzaman, E. Kwon, D. Y. Kim, Structural insights into the regulation of protein-arginine kinase McsB by McsA. *Proc. Natl. Acad. Sci. U. S. A.* **121**, e2320312121 (2024).
20. M. Darsonval, F. Julliat, T. Msadek, H. Alexandre, C. Grandvalet, CtsR, the Master Regulator of Stress-Response in Oenococcus oeni, Is a Heat Sensor Interacting With ClpL1. *Front. Microbiol.* **9**, 3135 (2018).
21. J. Hahn, N. Kramer, K. Briley Jr., D. Dubnau, McsA and B mediate the delocalization of competence proteins from the cell poles of Bacillus subtilis. *Mol. Microbiol.* **72**, 202−215 (2009).
22. J. Fuhrmann, V. Subramanian, D. J. Kojetin, P. R. Thompson, Activity-Based Profiling Reveals a Regulatory Link between Oxidative Stress and Protein Arginine Phosphorylation. *Cell Chem. Biol.* **23**, 967−977 (2016).
23. A. K. Elsholz *et al.*, CtsR inactivation during thiol-specific stress in low GC, Gram+ bacteria. *Mol. Microbiol.* **79**, 772−785 (2011).
24. S. Sitthisak *et al.*, McsA and the roles of metal-binding motif in Staphylococcus aureus. *FEMS Microbiol. Lett.* **327**, 126−133 (2012).
25. I. Derre, G. Rapoport, T. Msadek, CtsR, a novel regulator of stress and heat shock response, controls clp and molecular chaperone gene expression in gram-positive bacteria. *Mol. Microbiol.* **31**, 117−131 (1999).
26. I. Derre, G. Rapoport, K. Devine, M. Rose, T. Msadek, ClpE, a novel type of HSP100 ATPase, is part of the CtsR heat shock regulon of Bacillus subtilis. *Mol. Microbiol.* **32**, 581−593 (1999).
27. E. Kruger, M. Hecker, The first gene of the Bacillus subtilis clpC operon, ctsR, encodes a negative regulator of its own operon and other class III heat shock genes. *J. Bacteriol.* **180**, 6681−6688 (1998).
28. A. K. Elsholz, U. Gerth, M. Hecker, Regulation of CtsR activity in low GC, Gram+ bacteria. *Adv. Microb. Physiol.* **57**, 119−144 (2010).
29. I. Derre, G. Rapoport, T. Msadek, The CtsR regulator of stress response is active as a dimer and specifically degraded in vivo at 37 degrees C. *Mol. Microbiol.* **38**, 335−347 (2000).
30. A. K. Elsholz, S. Michalik, D. Zuhlke, M. Hecker, U. Gerth, CtsR, the Gram-positive master regulator of protein quality control, feels the heat. *EMBO J.* **29**, 3621−3629 (2010).
31. D. B. Trentini *et al.*, Arginine phosphorylation marks proteins for degradation by a

Clp protease. *Nature* **539**, 48−53 (2016).
32. A. A. Hoskins *et al.*, Ordered and dynamic assembly of single spliceosomes. *Science* **331**, 1289−1295 (2011).
33. T. Ha *et al.*, Probing the interaction between two single molecules: fluorescence resonance energy transfer between a single donor and a single acceptor. *Proc. Natl. Acad. Sci. U. S. A.* **93**, 6264–6268 (1996).
34. T. Ha *et al.*, Initiation and re-initiation of DNA unwinding by the Escherichia coli Rep helicase. *Nature* **419**, 638–641 (2002).
35. C. J., Fischer, N. K. Maluf, T. M. Lohman, Mechanism of ATP-dependent translocation of E. coli UvrD monomers along single-stranded DNA. *J. Mol. Biol.* **344**, 1287−1309 (2004).
36. H. Hwang, H. Kim, S. Myong, Protein induced fluorescence enhancement as a single molecule assay with short distance sensitivity. *Proc. Natl. Acad. Sci. U. S. A.* **108**, 7414−7418 (2011).
37. B. Hua *et al.*, The Single-Molecule Centroid Localization Algorithm Improves the Accuracy of Fluorescence Binding Assays. *Biochemistry* **57**, 1572−1576 (2018).
38. J. Abramson *et al.*, Accurate structure prediction of biomolecular interactions with AlphaFold 3. *Nature* **630**, 493−500 (2024).
39. D. S. White, M. A. Smith, B. Chanda, R. H. Goldsmith, Strategies for Overcoming the Single-Molecule Concentration Barrier. *ACS Meas. Sci. Au* **3**, 239−257 (2023).
40. F. Rashid *et al.*, Initial state of DNA-Dye complex sets the stage for protein induced fluorescence modulation. *Nat. Commun.* **10**, 2104 (2019).
41. J. Fuhrmann *et al.*, Structural Basis for Recognizing Phosphoarginine and Evolving Residue-Specific Protein Phosphatases in Gram-Positive Bacteria. *Cell Rep.* **3**, 1832–1839 (2013).
42. Z. Zhang, K. M. Dubiak, P. W. Huber, N. J. Dovichi, Miniaturized Filter-Aided Sample Preparation (MICRO-FASP) Method for High Throughput, Ultrasensitive Proteomics Sample Preparation Reveals Proteome Asymmetry in Xenopus laevis Embryos. *Anal. Chem.* **92**, 5554–5560 (2020).
43. I. Rasnik, S. A. McKinney, T. Ha, Nonblinking and long-lasting single-molecule fluorescence imaging. *Nat. Methods* **3**, 891–893 (2006).
44. B. Hua *et al.*, An improved surface passivation method for single-molecule studies. *Nat. Methods* **11**, 1233−1236 (2014).

Figures

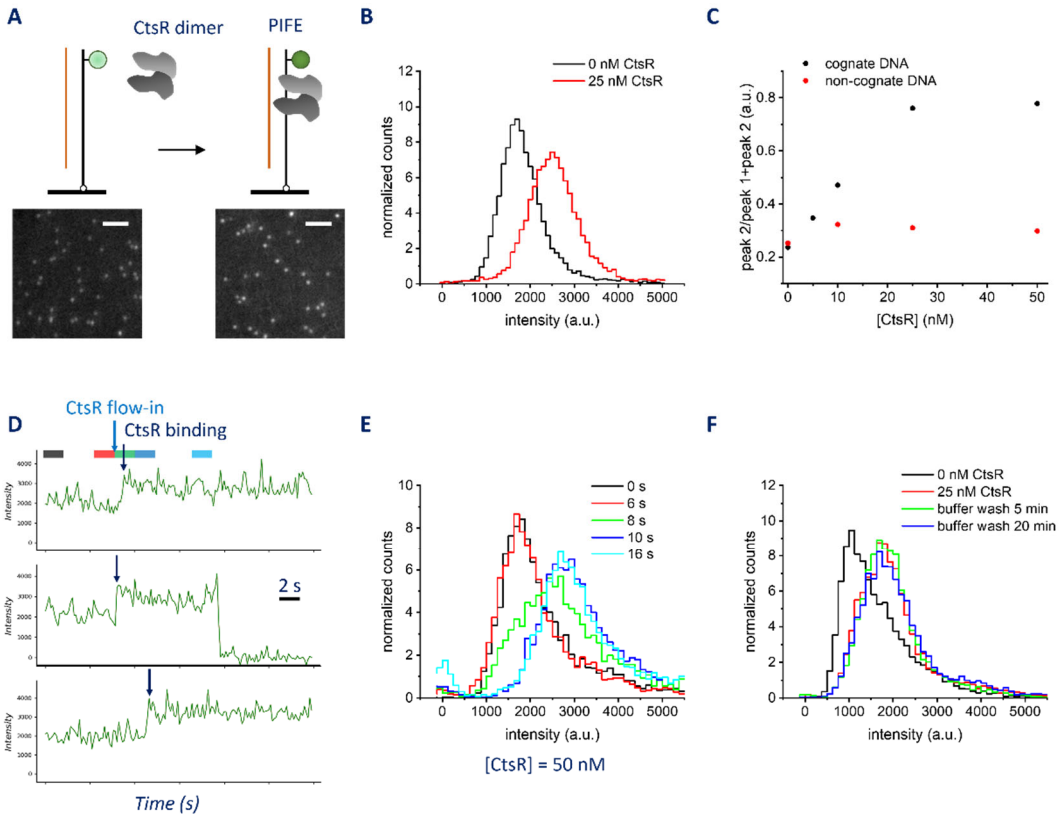

Figure 1. Single-molecule analysis of the CtsR-DNA interaction. (A) Schematic showing the fluorescently labeled DNA probe for monitoring CtsR binding based on the PIFE effect. Inserts are representative images of single DNA probes before and after CtsR binding. The scale bars correspond to 2.5 μm. (B) Fluorescence intensity histograms of the DNA probe alone (black) and bound by 25 nM CtsR (red). (C) The fraction of CtsR-bound DNA as a function of the protein concentration in solution. Black dots represent the cognate DNA, whereas the red dots represent the non-cognate DNA. (D) Example fluorescence intensity trajectories of real-time CtsR binding to the target DNA upon the addition of 50 nM CtsR in the flow cell. The scale bar corresponds to 2 s in time. (E) Time-dependent fluorescence intensity histograms constructed from the acquired trajectories at different time points as indicated by the colored segments in (D). (F) Fluorescence intensity histograms of the CtsR-DNA complex before and at different time points after a buffer wash to remove the excess CtsR in solution.

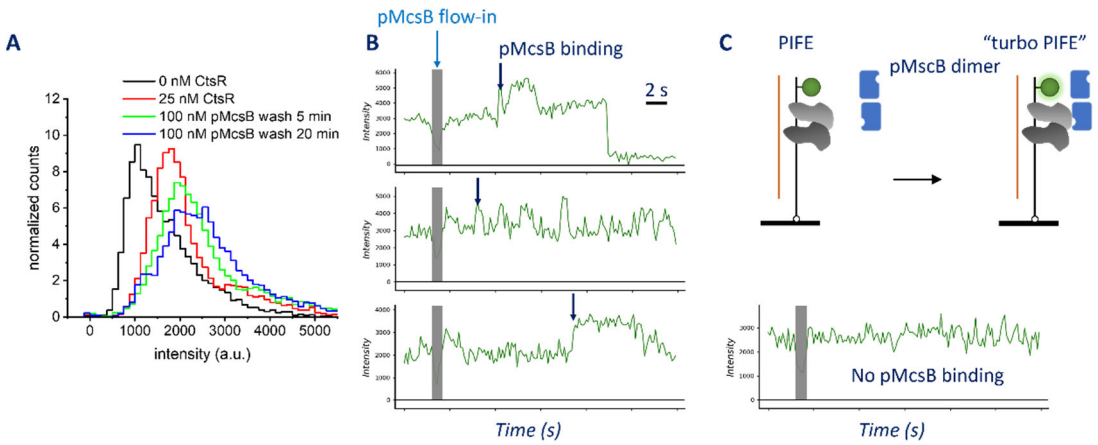

Figure 2. Single-molecule analysis of the pMcsB-CtsR-DNA interaction. (A) Fluorescence intensity histograms of the CtsR-DNA complex before and at different time points after a pMcsB and ATP wash to remove the excess CtsR in solution. (B-C) Example fluorescence intensity trajectories of real-time pMcsB binding to the CtsR-DNA complex upon the addition of 200 nM pMcsB and 0.5 mM ATP in the flow cell. The scale bar corresponds to 2 s in time. In many trajectories, transient spikes were observed indicating pMcsB binding to the CtsR-DNA complex, while some trajectories did not show such events. (C) Schematic showing pMcsB binding to the CtsR-DNA complex as monitored by the "turbo PIFE" effect.

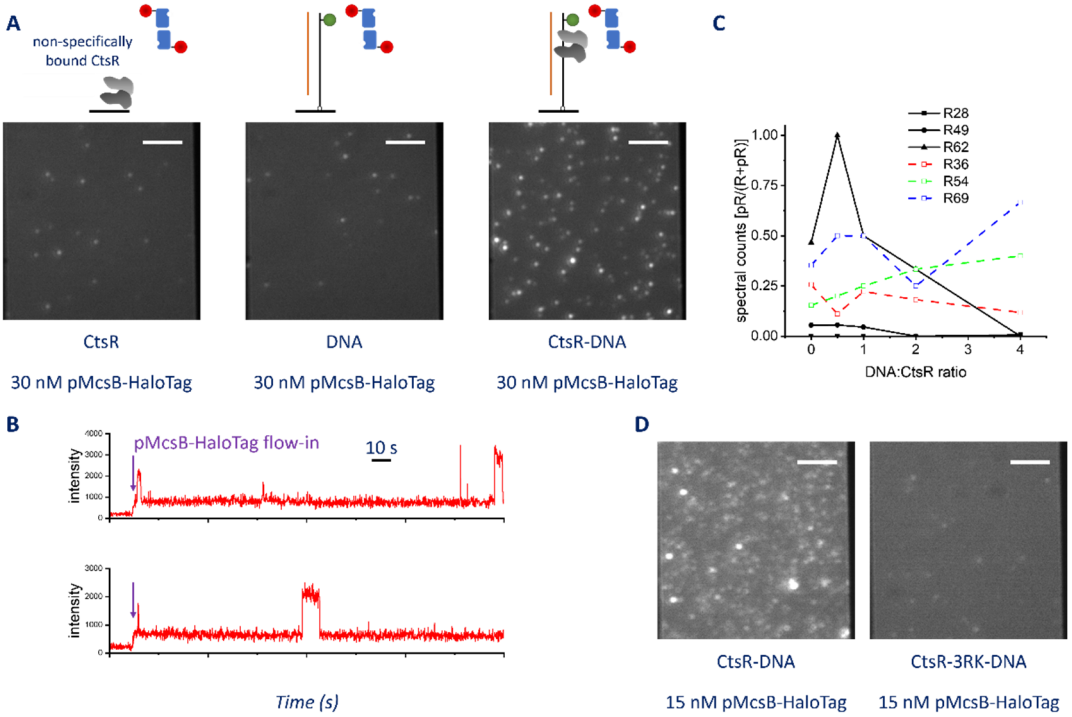

Figure 3. Single-molecule analysis of the pMcsB-HaloTag-CtsR-DNA interaction. (A) Fluorescence images of the AS RED-labeled pMcsB-HaloTag interacting with non-specifically bound CtsR (left), the DNA probe alone (middle) and the CtsR-DNA complex (right). The scale bars correspond to 5 μm. (B) Example fluorescence intensity trajectories of real-time pMcsB-HaloTag binding to the CtsR-DNA complex upon the

addition of 15 nM pMcsB-HaloTag and 0.5 mM ATP in the flow cell. The scale bar corresponds to 10 s in time. The trajectories are extracted from analyzing the integrated intensity at each frame in a single-molecule movie. (C) The relative spectral counts (phosphorylated peptides/total peptides) for positions 28, 49, 62, 36, 54 and 69 at different DNA:CtsR ratios. (D)Fluorescence images of the AS RED-labeled pMcsB-HaloTag interacting with the wild-type CtsR-DNA complex (left) and the mutant CtsR-3RK-DNA complex (right). The scale bars correspond to 5 μm.

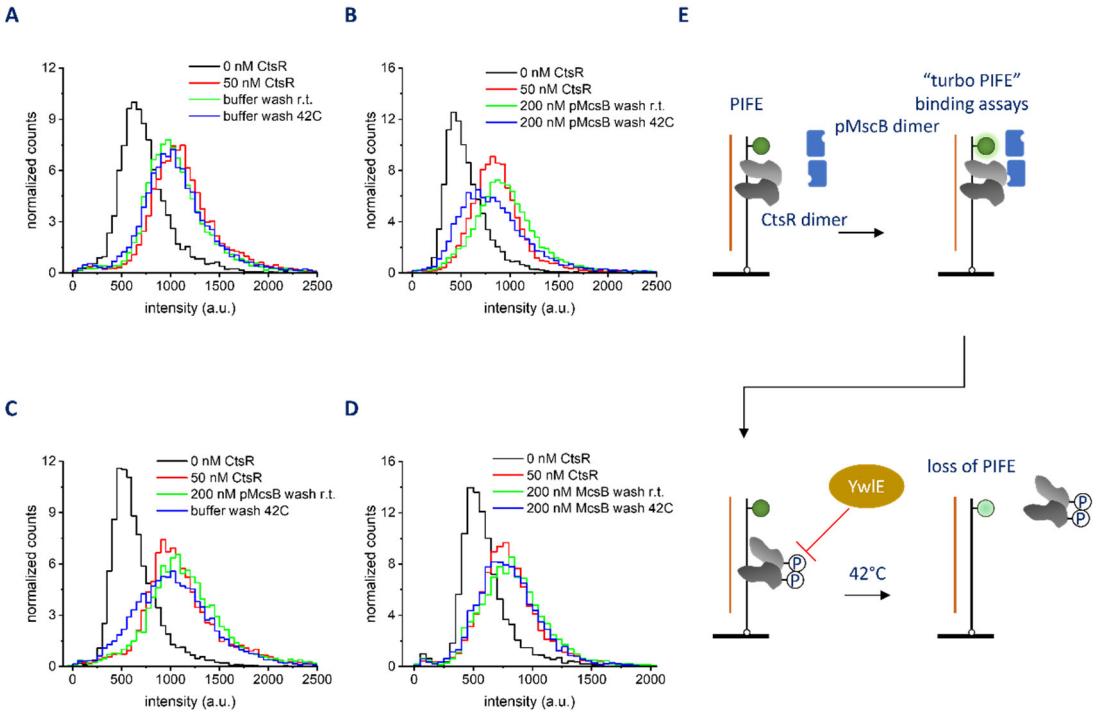

Figure 4. Temperature and phosphorylation-induced CtsR dissociation. (A) Fluorescence intensity histograms of the CtsR-DNA complex before and after a buffer wash at 42˚C. The complex was incubated in the buffer for 10 min at room temperature before the heated wash. (B) Fluorescence intensity histograms of the CtsR-DNA complex before and after a pMcsB and ATP wash at 42˚C. The complex was first treated with pMcsB and ATP for 10 min at room temperature before the heated wash. (C) Fluorescence intensity histograms of the CtsR-DNA complex before and after a buffer wash at 42˚C. The complex was first treated with pMcsB and ATP for 10 min at room temperature before the heated wash. (D) Fluorescence intensity histograms of the CtsR-DNA complex before and after a McsB wash in the absence of ATP at 42˚C. The complex was first treated with McsB in the absence of ATP for 10 min at room temperature before the heated wash. r.t. in (A-D) stands for room temperature. (E) Schematic showing that the balance of McsB and YwlE influences the phosphorylation states and the heat sensitivity of the CtsR-DNA complex.

Supplementary figures

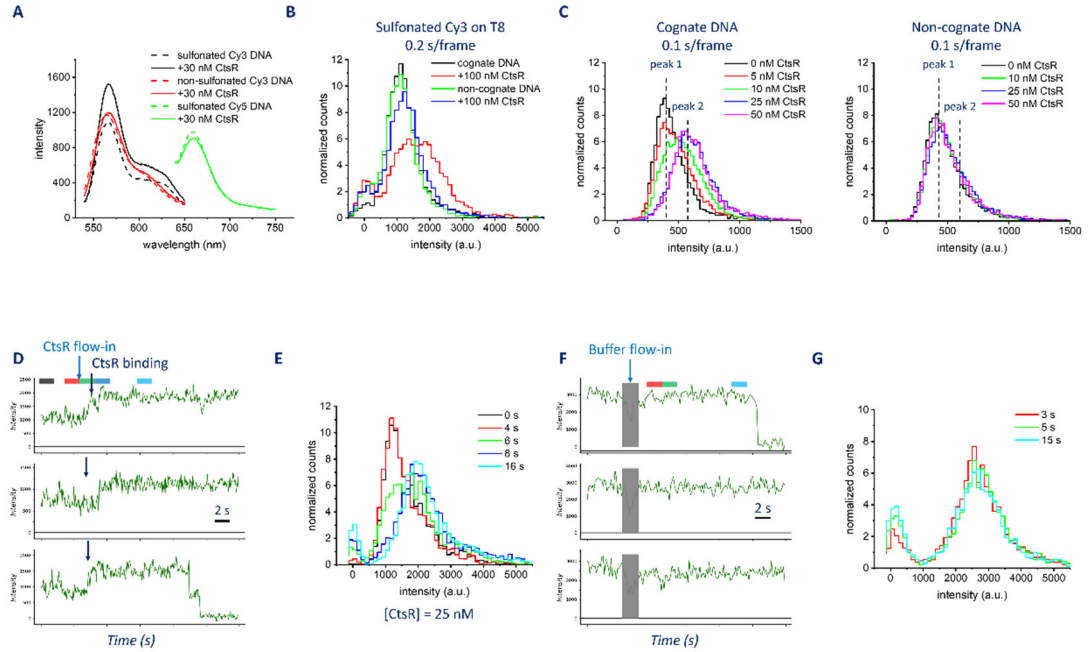

Supplementary Figure 1. Single-molecule analysis of the CtsR-DNA interaction. (A) Bulk fluorescence measurements of the PIFE effects from DNA probes labeled with different fluorophores. While sulfonated Cy3 showed a ~1.5-fold fluorescence enhancement, the non-sulfonated Cy3 and sulfonated Cy5 did not show any PIFE effect. (B) Fluorescence intensity histograms of a DNA probe with sulfonated Cy3 labeled at the T8 position. Labeling the fluorophore at T8 (instead of T9) on the DNA weakened CtsR binding, as it was only partially bound by CtsR at 100 nM protein concentration. (C) Fluorescence intensity histograms of the cognate (left) and non-cognate (right) DNA probes at different concentrations of CtsR. (D) Example fluorescence intensity trajectories of real-time CtsR binding to the target DNA upon the addition of 25 nM CtsR in the flow cell. The scale bar corresponds to 2 s in time. The frame rate was 0.1 s/frame. (E) Time-dependent fluorescence intensity histograms constructed from the acquired trajectories at different time points as indicated by the colored segments in (D). (F) Example fluorescence intensity trajectories of the CtsR-DNA complex upon washing away the excess CtsR in solution. The scale bar corresponds to 2 s in time. The frame rate was 0.2 s/frame. (G) Time-dependent fluorescence intensity histograms constructed from the acquired trajectories at different time points as indicated by the colored segments in (F).

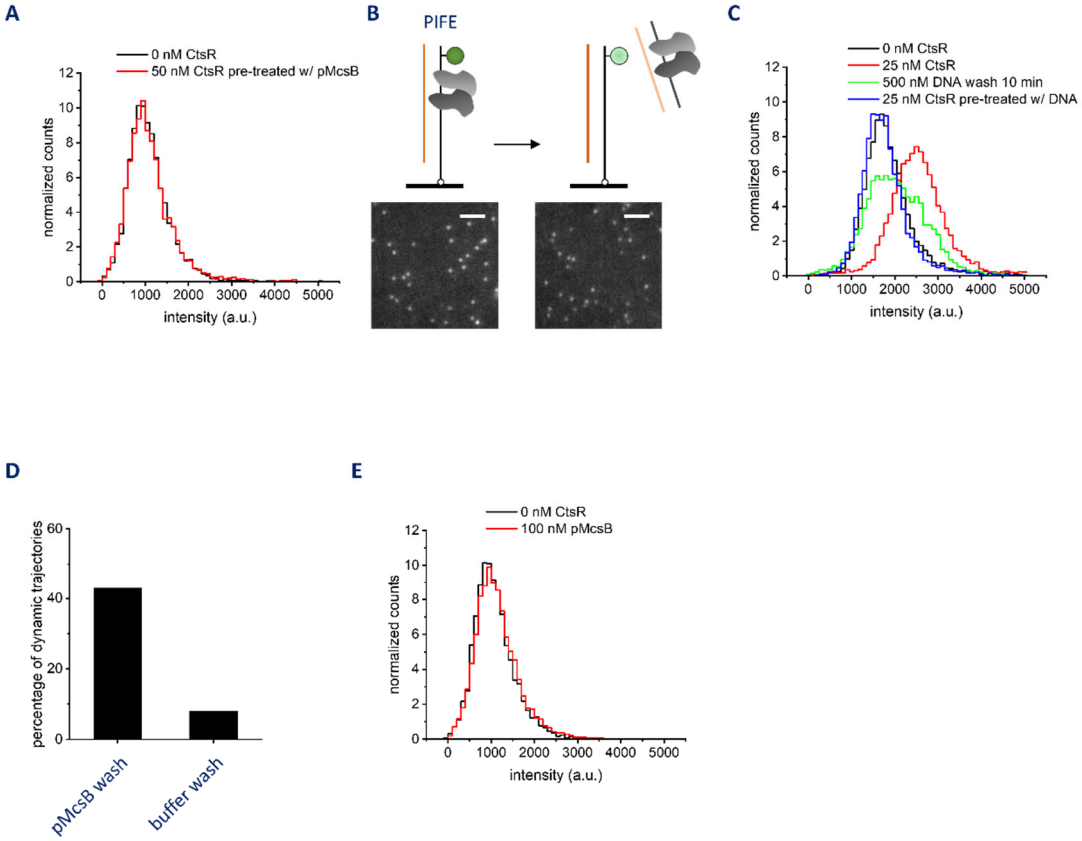

Supplementary Figure 2. Single-molecule analysis of the pMcsB-CtsR-DNA interaction. (A) Fluorescence intensity histograms of the DNA probe alone (black) and incubated with 50 nM pre-treated CtsR (red). CtsR was pre-treated with 200 nM pMcsB and 0.5 mM ATP for 15 min before the protein was added to the flow cell. (B) Schematic showing the cognate DNA in solution competing off the bound CtsR as monitored by the loss of PIFE effect. Inserts are representative images of single DNA probes before and after CtsR competing-off. The scale bars correspond to 2.5 μm. (C) Fluorescence intensity histograms of the DNA probe alone (black), bound by 25 nM CtsR (red), after CtsR competing-off (green) and 25 nM CtsR pre-bound with the cognate DNA (blue). When CtsR was pre-bound with the cognate DNA in solution, it cannot bind to the surface-tethered cognate DNA. (D) The percentage of trajectories showing transient spikes after the pMcsB and buffer washes, respectively. (E) Fluorescence intensity histograms of the DNA probe alone (black) and incubated with 100 nM pMcsB and 0.5 mM ATP (red).

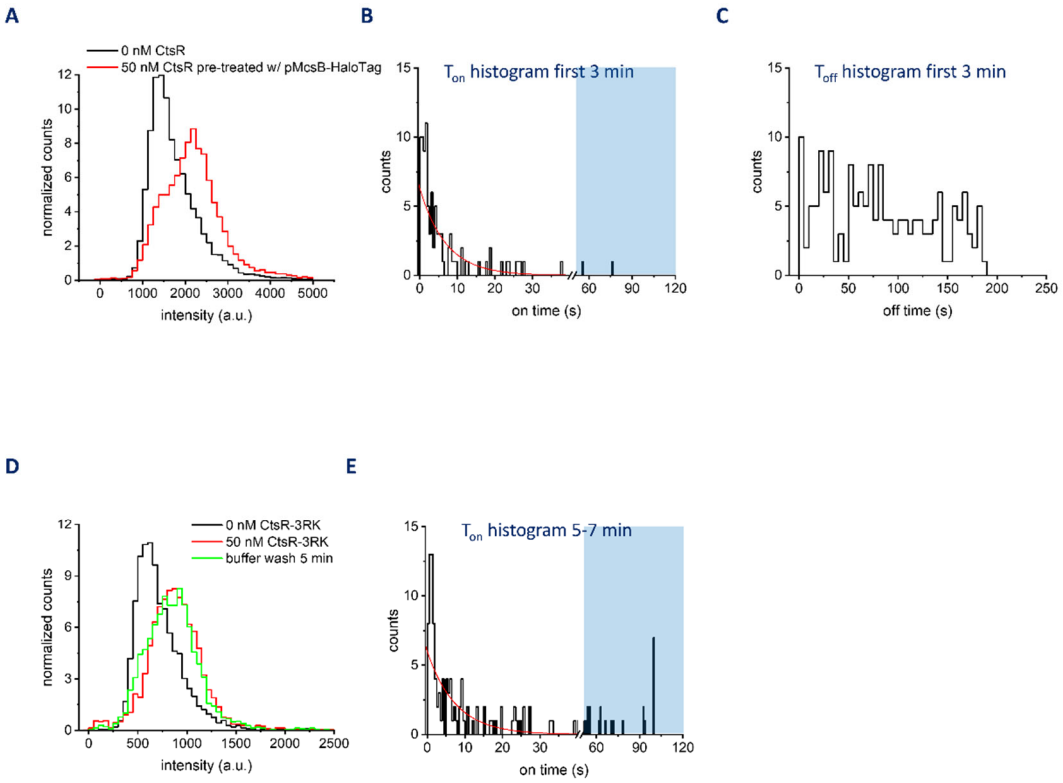

Supplementary Figure 3. Single-molecule analysis of the pMcsB-HaloTag-CtsR-DNA interaction. (A) Fluorescence intensity histograms of the DNA probe alone (black) and incubated with 50 nM pre-treated CtsR (red). CtsR was pre-treated with 200 nM pMcsB-HaloTag and 0.5 mM ATP for 15 min before the protein was added to the flow cell. (B-C) Dwell time histograms of the pMcsB-HaloTag-bound durations (T_{on}, B) and unbound durations (T_{off}, C). The dwell times were collected in the first 3 min after the addition of pMcsB-HaloTag in the flow cell. (D) Fluorescence intensity histograms of the mutant CtsR-3RK-DNA complex before and 5 min after a buffer wash to remove the excess CtsR-3RK in solution. (E) A dwell time histogram of the pMcsB-HaloTag-bound durations (T_{on}). The dwell times were collected 5-7 min after the addition of pMcsB-HaloTag in the flow cell.

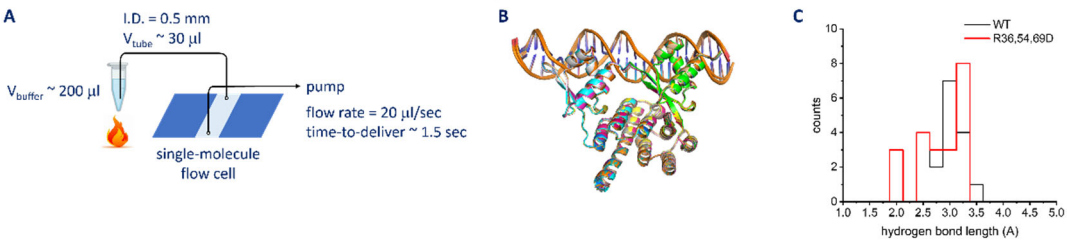

Supplementary Figure 4. Structural predictions and analysis of the CtsR-DNA complexes. (A) Schematic showing the device for the heated buffer washes. (B) Structure alignment of the CtsR-DNA complexes. (C) Hydrogen bond length histograms of the wild-type (black) and R36,54,69D (red) CtsR-DNA complexes.